PAPER

Check for updates

High CO$_2$ separation performance on a metal–organic framework composed of nano-cages lined with an ultra-high density of dual-side open metal sites†

Liangjun Li, [iD] ‡*[a] Jiangxiu He,‡[ab] Wenli Xu,[a] Kuitong Zhang,[c] Tao Xing,[c] Zhi Li,[cd] Dewen Zhen,*[e] Bo Xiong,[e] Zhixing Ge,[e] Xi Zhang,[e] Shanyu Wang,[e] Fuzhao Zhang,[a] Xin Gu, [iD] [a] Pengcheng Dai, [iD] [a] Dandan Liu,[a] Lingzhi Yang [iD] [a] and Xuebo Zhao [iD] *[a]

Developing efficient adsorbents for CO$_2$ separation is the crucial step of CO$_2$ sequestration. which has found many applications, including in carbon capture from flue gas and natural gas purification. Although many adsorbents have been reported in the past few decades, developing efficient adsorbents with high separation selectivity and excellent capacity is technically challenging due to the trade-off effect between the adsorption capacity and selectivity. This work reports the CO$_2$ separation performance of a microporous MOF, which comprises nano-cages and an ultra-high density of dual-side open metal sites. The adsorption results reveal a prominent CO$_2$ uptake and outstanding separation selectivity for CO$_2$/N$_2$ and CO$_2$/CH$_4$. Furthermore, this MOF also exhibits the preferable adsorption of C2–C3 light hydrocarbons over CH$_4$. Simulation studies reveal that the dual-side open metal sites are the preferable adsorption sites for CO$_2$, C$_2$H$_4$, and C$_3$H$_6$. Therefore, the outstanding separation performance can be attributed to the combined effects of nano-cages and the high density of open metal sites.

Introduction

With the increasing concern over global warming, the reduction of carbon emissions into the atmosphere has been a focus worldwide.[1] Generally, there are two major routes of reducing carbon dioxide emissions. First, carbon capture and sequestration (CCS) from flue gas is the primary strategy to minimize human carbon emissions in the current stage.[2,3] Second, replacing the high-carbon energy source (such as petroleum, coal, *etc.*) with a low-carbon energy source (such as CH$_4$, H$_2$, *etc.*) is the ultimate solution to carbon reduction.[4,5] Regarding CO$_2$ capture, CO$_2$ separation from gas mixtures

through pressure swing adsorption (PSA) has been regarded as an alternative technique of CO$_2$ separation to the conventional chemical absorption process, which is energy-intensive and corrosive.[6–9] The advantages, such as high energy efficiency, low plant investments, and easy mobility, render this technique with very promising potential for CO$_2$ capture.[10,11] Besides, the separation of CO$_2$ from natural gas is central to natural gas production due to its incredible relevance to energy value and transportation safety.[12,13] As an alternative technique to the conventional cryogenic distillation process that is energy and cost-intensive, the physisorption-based PSA process has been the most promising strategy for CO$_2$/CH$_4$ separation due to its low energy consumption and low investments.[14,15]

The adsorbent is the core material for the PSA process that determines the separation efficiency and energy cost. Metal–organic frameworks (MOFs) represent an emerging family of crystalline adsorbents with a uniform structure, amenable pore environments, and tuneable functionalities among various adsorbents.[16,17] Besides their encouraging prospects in a wide range of applications, they are also considered as ideal adsorbents for CO$_2$ separation.[18,19] In the past two decades, various MOFs with high CO$_2$ separation selectivities have been reported. However, constructing MOFs with high separation CO$_2$ selectivity and excellent capacity is still challenging and urgent. This work reports the separation performance of a MOF

[a] *Department of Energy Storage Science and Engineering, College of New Energy, China University of Petroleum (East China), Qingdao, 266580, China. E-mail: lilj@upc.edu.cn, Zhaoxuebo@upc.edu.cn*

[b] *Sinopec Qingdao Petrochemical Co., Ltd., Qingdao, 266580, China*

[c] *New Energy Division, Shandong Energy Group Co., Ltd. Zoucheng, Jining, China*

[d] *School of Materials Science and Engineering, Xi'an Jiaotong University, Xi'an, 710049, China*

[e] *New Energy Department, Research Institute of Petroleum Exploration & Development, China National Petroleum Corporation, Langfang, 065007, China. E-mail: zdw69@petrochina.com.cn*

† Electronic supplementary information (ESI) available: Synthetic details, crystal structural parameters, PXRD pattern, calculation procedures and additional kinetic profiles. See DOI: 10.1039/d1ma00919b

‡ These authors contributed equally to this work.

composed of nano-cages lined with a high density of dual-side open metal sites. The gas adsorption study reveals both high adsorption capacity and excellent separation selectivity for CO_2. Theoretical studies and breakthrough experiments also validate the effectiveness of this strategy in promoting the separation efficiency for CO_2 capture from flue gas and natural gas.

Results and discussion

To construct a MOF with multiple functionalities, employing a multiple-functional ligand is the most direct method. 1H-pyrazole-4-carboxylic acid (H_2PCA) is the simplest multiple-functional ligand composed of carboxylate and pyrazole groups. Through the solvothermal reaction of H_2PCA and Cu^{2+} ions, a three-dimensional porous MOF with nano-cages was obtained (see Experimental details in the ESI,† S1). Deep blue block-like single crystals with a homogeneous morphology were obtained in a high yield. Single-crystal X-ray diffraction analysis reveals a three-dimensional network with a formula of $[Cu_3(\mu_3\text{-OH})(PCA)_3]$. The structural retrieval shows that the crystal structure of this MOF has been reported in former literature.[20] However, the gas adsorption properties of this MOF have not been reported yet.

This MOF is crystallized in a high symmetrical cubic system, with a space group of $F\bar{4}3c$. The coordination of three pyrazole groups with three Cu^{2+} ions and one bridging oxygen atom gives rise to triangle trinuclear $[Cu_3(\mu_3\text{-OH})(PCA)_3]$ secondary building units (SBUs) (see Fig. 1a and b). The $[Cu_3(\mu_3\text{-OH})(Pz)_3]$ (Pz represents pyrazole) group in this SBU is a commonly encountered coordination sphere created by pyrazole and transition metal ions. Other than forming the $[Cu_3(\mu_3\text{-OH})(PCA)_3]$ SBU, the Cu(ɪɪ) atom is also coordinated to the carboxylate group on another $[Cu_3(\mu_3\text{-OH})(PCA)_3]$ group, giving rise to a planar square coordination environment for Cu(ɪɪ). Notably, a high density of open metal sites on SBUs can be formed directly without evacuating the coordinated water molecules. Structural analysis reveals that nano-cages with a diameter of 0.97 nm and windows with a diameter of 0.38 nm are involved in this MOF, with a high porosity of 47% calculated from the PLANTON[21] program (see Fig. 1c–e).

The PXRD pattern of the sample prepared from a scale-up experiment is consistent well with the pattern simulated from the single-crystal data, suggesting that this sample possesses the same structure with $[Cu_3(\mu_3\text{-OH})(PCA)_3]$ and has a high degree of crystallinity (as shown in Fig. 1e). Thermal gravimetric analysis (TGA) reveals that this MOF is stable up to 270 °C (see TGA curves in the ESI,† S2). After thermal activation at 130 °C, N_2 adsorption at 77 K was performed on this sample. As shown in Fig. 1f, the typical type-I isotherm indicates the microporous nature of this MOF, which is agreeable with the crystallographic data. The BET surface area derived from the N_2 isotherm is 583 $m^2 g^{-1}$, with a pore volume of 0.249 $cm^3 g^{-1}$.

Owing to the square planar coordination geometry for Cu(ɪɪ) and unique configuration, the dual sides of each Cu(ɪɪ) center are exposed in the nano-cages, leading to a relatively high density of accessible open metal sites for this MOF. The density of accessible open metal sites is calculated to be 28 nm^{-3}, much higher than the famous MOFs with a high density of open metal sites, such as HKUST-1 (10.5 nm^{-3}) and MOF-74 (4.6 nm^{-3}). Besides, the nitrogen atoms in the ligand and oxygen atoms in the carboxylate groups could act as additional active sites for gas adsorption. The combination of nano-cages and the high density of open metal sites render this MOF a promising material for CO_2 capture.

The isotherms of CO_2, N_2, and CH_4 at ambient temperatures were measured on the activated sample of $[Cu_3(\mu_3\text{-OH})(PCA)_3]$ to investigate its gas adsorption properties. As shown in Fig. 2a, $[Cu_3(\mu_3\text{-OH})(PCA)_3]$ exhibits a CO_2 uptake of 2.93 mmol g^{-1} (65.6 $cm^3 g^{-1}$) at 1 bar and 298 K. With increasing temperature, the CO_2 uptake gradually decreases. In contrast to the high uptake of CO_2, $[Cu_3(\mu_3\text{-OH})(PCA)_3]$ exhibits a near-linear N_2 isotherm and displays a negligible uptake of N_2 at 298 K (as shown in Fig. 2b). The significant difference between the isotherms of CO_2 and N_2 indicates the high adsorption selectivities for CO_2/N_2. Similar to N_2, $[Cu_3(\mu_3\text{-OH})(PCA)_3]$ also displays a linear isotherm for CH_4 at 298 K, exhibiting a CH_4 uptake of 0.67 mmol g^{-1} at 298 K and 1 bar.

Based on CO_2 isotherms at different temperatures, the CO_2 adsorption enthalpy (Q_{st}) was calculated by using the Clausius–Clapeyron relation (see the calculated procedure in the ESI,† S3). As shown in Fig. 2c, the Q_{st} of CO_2 adsorption is in the range of 31.5–36.1 kJ mol^{-1}, with minor differences with increasing adsorption amounts. These Q_{st} values are apparently larger than that of common MOFs, such as HKUST-1 (25.26 kJ mol^{-1})[22] and NiDABCO (20 kJ mol^{-1}).[23] The large value of Q_{st} suggests the high adsorption potential of $[Cu_3(\mu_3\text{-OH})(PCA)_3]$ to CO_2 molecules. The high adsorption potentials to CO_2 molecules could be attributed to the synergistic effect of nano-cages and the high density of open metal sites.

Based on adsorption isotherms, the equilibrium adsorption selectivity for the CO_2/N_2 mixture can be evaluated by the ideal adsorbed solution theory (IAST), of which several studies have widely validated the reliability.[10,24] As shown in Fig. 2d, the IAST selectivity for the CO_2/N_2 mixture is calculated as 70 at 1 bar and 298 K (see calculation procedures in the ESI,† S4). This value is among the high ranks of adsorbents and is significantly higher than that of the common MOFs (see comparison Table in the ESI,† S5).[18] Induced by the higher adsorption potential for CO_2, $[Cu_3(\mu_3\text{-OH})(PCA)_3]$ shows a high CO_2/CH_4 selectivity. The equilibrium CO_2/CH_4 selectivity calculated from IAST is in the range of 11.8–15.9, which is also superior to the bench-marking MOFs, such as HKSUT-1 (5.5)[18,22] and NiDABCO.[23]

The outstanding CO_2 separation performance of $[Cu_3(\mu_3\text{-OH})(PCA)_3]$ also encourages us to investigate the separation performance for light hydrocarbons, which play crucial roles in petroleum chemistry. As shown in Fig. 2e, $[Cu_3(\mu_3\text{-OH})(PCA)_3]$ exhibits type-I isotherms for C_2H_4, C_2H_6, C_3H_6, and C_3H_8, which is in clear contrast with CH_4. At 298 K and 1 bar, adsorption uptakes of 2.2, 1.9, 2.5, and 2.1 mmol g^{-1} are observed for C_2H_4, C_2H_6, C_3H_6, and C_3H_8, respectively. We can clearly see that the
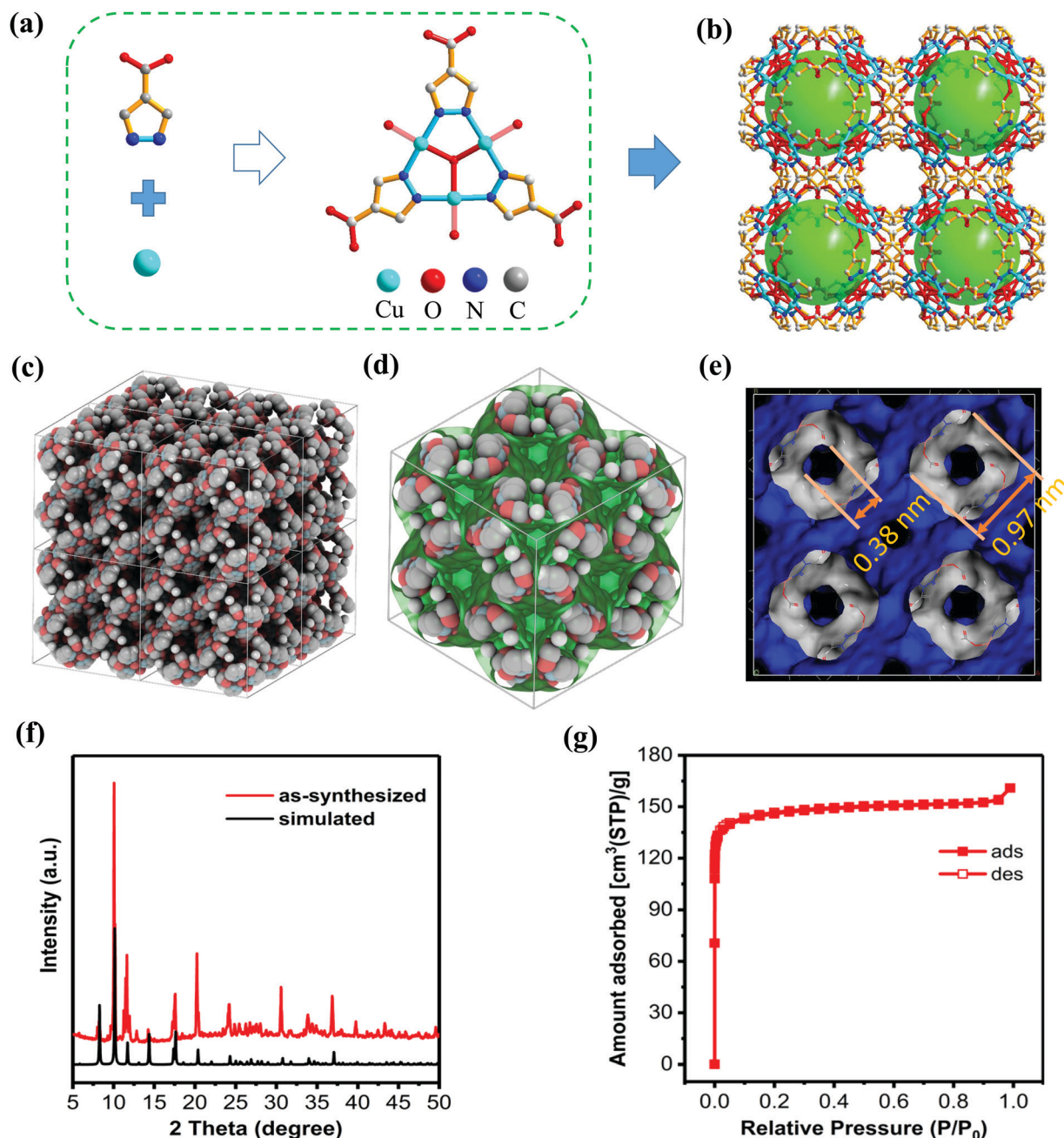
Fig. 1 (a) Illustration of the formation process, ligand and tri-nuclear secondary building units of [Cu₃(μ₃-OH)(PCA)₃]; (b) the perspective view of the crystallographic structure of [Cu₃(μ₃-OH)(PCA)₃] along the *c* axis exhibiting the nano-cages and channels; (c) the packing mode presentation of [Cu₃(μ₃-OH)(PCA)₃] displaying the pore structures; (d) the adsorption surface calculated (green colour) using the He molecules as the probe viewing from the (111) direction; (e) the Connolly surface calculated using a probe radius of 1.0 Å illustrating the accessible nano-cages and windows in [Cu₃(μ₃-OH)(PCA)₃]; (f) the comparison between the powder X-ray diffraction and simulated XRD patterns; and (g) the N₂ isotherm performed at 77 K.

adsorption uptake increases with the chain length of light hydrocarbons. Furthermore, the adsorption uptakes of C_2H_4 and C_3H_6 are higher than those of C_2H_6 and C_3H_8, implying that alkenes are more preferentially adsorbed on [Cu₃(μ₃-OH)(PCA)₃] than alkanes. Based on the isotherms at different temperatures, the Q_{st} values of adsorption for C_2H_4, C_2H_6, C_3H_6, and C_3H_8 are calculated as 35.4, 33.8, 54.6, and 45.8 kJ mol^{-1}, respectively. The higher Q_{st} values for C3 molecules compared to C2 molecules indicate that [Cu₃(μ₃-OH)

(PCA)₃] displays a higher interaction strength with the hydrocarbons with longer chain length. Besides, [Cu₃(μ₃-OH)(PCA)₃] shows a higher interaction strength with alkenes than alkanes. The preferential adsorption of alkenes to alkanes could be attributed to the π-electrons of alkenes, which could give back donations to open metal sites of MOFs. Due to the higher adsorption potentials, [Cu₃(μ₃-OH)(PCA)₃] exhibits higher adsorption selectivity for C2/C3 hydrocarbons than CH_4. Based on their adsorption isotherms, the equilibrium adsorption selectivities for
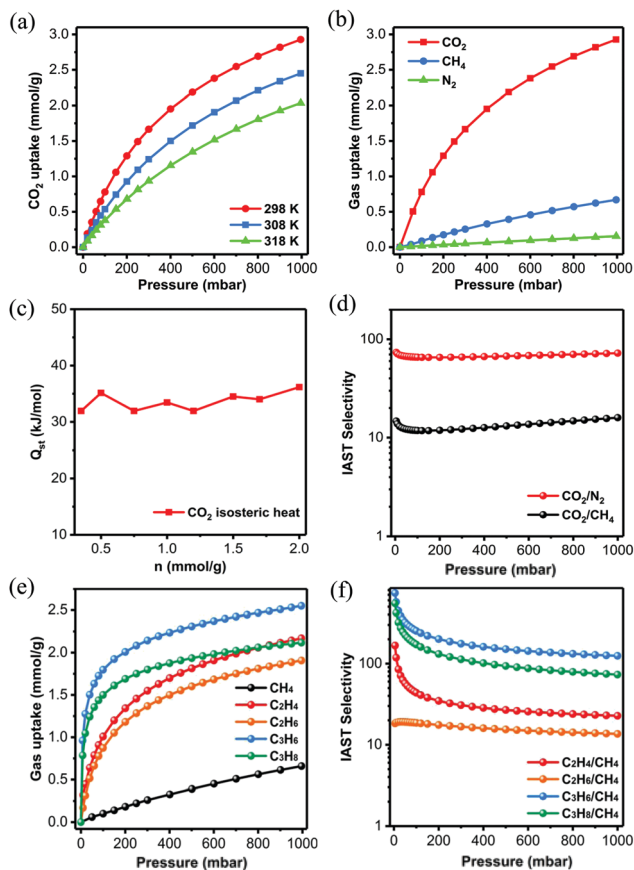
Fig. 2 (a) CO_2 adsorption isotherms on [$Cu_3(\mu_3$-OH)(PCA)$_3$] at 298, 308 and 318 K and 0–1 bar; (b) the comparison of adsorption isotherms for CO_2, CH_4 and N_2 on [$Cu_3(\mu_3$-OH)(PCA)$_3$] at 298 K; (c) the isosteric adsorption enthalpy for CO_2 adsorption on [$Cu_3(\mu_3$-OH)(PCA)$_3$]; (d) the equilibrium separation selectivity for CO_2/N_2 and CO_2/CH_4 mixtures calculated from the IAST method at a feed gas ratio of 50/50; (e) the comparison of adsorption isotherms for CH_4, C_2H_4, C_2H_6, C_3H_6 and C_3H_8 on [$Cu_3(\mu_3$-OH)(PCA)$_3$] at 298 K; (f) the equilibrium separation selectivity for equimolar C_2H_4/CH_4, C_2H_6/CH_4, C_3H_6/CH_4 and C_3H_8/CH_4 mixtures calculated from the IAST method.

C_2H_4/CH_4, C_2H_6/CH_4, C_3H_6/CH_4, and C_3H_8/CH_4 at 298 K are in the range of 22–167, 13–18, 124–737, and 73–550, respectively (as shown in Fig. 2f). Notably, at 298 K and 1 bar, high IAST selectivities of 124 and 73 have been reached for C_3H_6/CH_4 and C_3H_8/CH_4, outperforming common adsorbents and common MOFs.[25,26] The excellent adsorption uptake and separation selectivity demonstrates the promising potential of [$Cu_3(\mu_3$-OH)(PCA)$_3$] in separating light hydrocarbons.

To investigate the separation mechanism, the Grand canonical Monte Carlo (GCMC)[27] simulations for CO_2, CH_4, C_2H_4, and C_2H_6 adsorption on [$Cu_3(\mu_3$-OH)(PCA)$_3$] were performed (as shown in Fig. 3). It is clearly shown that CO_2 molecules are concentrated near the tri-nuclear open metal sites, and the density of CO_2 molecules near open metal sites is much higher than other sites. This phenomenon demonstrates that these open metal sites are the preferred adsorption sites for CO_2. Compared to CO_2, the CH_4 molecules are more dispersed in the pore space, and the density near the open metal sites is much lower. This comparison result
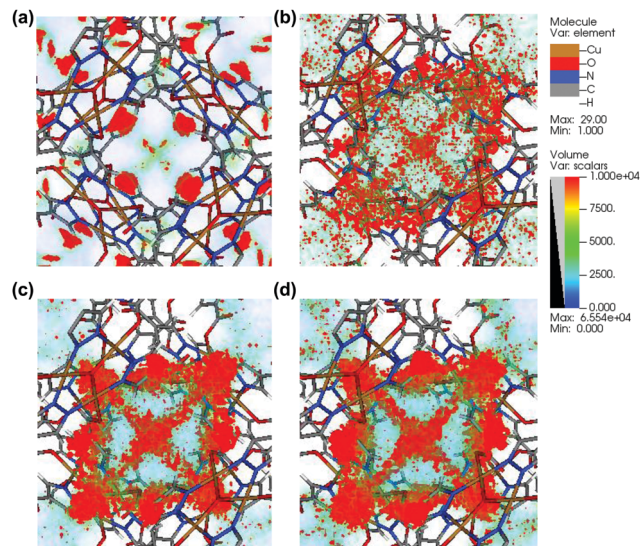
Fig. 3 (a) Density distribution of guest molecules within [$Cu_3(\mu_3$-OH)(PCA)$_3$] for: (a) CO_2; (b) CH_4; (c) C_2H_4; (d) C_2H_6. (The density distribution was calculated at 298 K and 1 bar using the GCMC method.)

suggests the pronounced function of open metal sites in CO_2 adsorption. Like CO_2, the open metal sites exert high adsorption potentials to C_2H_4 and C_2H_6, which is agreeable with the experimental results. The density distributions of C_2H_4 and C_2H_6 molecules are much higher than CH_4, indicating the preferable adsorption of C_2H_4 and C_2H_6 over CH_4 molecules. The simulation results also confirm the effectiveness of incorporating a high density of open metal sites in enhancing the separation performance of MOFs.

To validate the actual separation performance of [$Cu_3(\mu_3$-OH)(PCA)$_3$], the breakthrough experiments were performed on the column packed with [$Cu_3(\mu_3$-OH)(PCA)$_3$] (as shown in Fig. 4). At a feed gas ratio of 50/50 and the pressure of 1 bar, N_2 quickly breaks through from the packed column, while CO_2 requires a rather long time to elute from the column (see Fig. 4a). The significant distinction in the breakthrough time of reaching the outlet of the packed column suggests that [$Cu_3(\mu_3$-OH)(PCA)$_3$] is capable of separating the mixed CO_2/N_2 (50/50) gas completely. Similarly, CO_2 and CH_4 also exhibit a remarkable difference in times of breaking through from the pack column at a feed gas
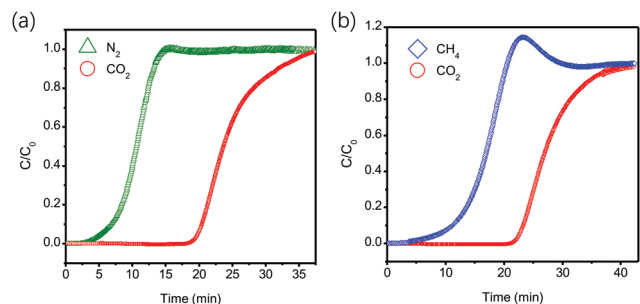
Fig. 4 (a) Experimental column breakthrough curves for (a) CO_2 and N_2 mixtures (50/50, v/v) and (b) CO_2 and CH_4 mixtures (50/50, v/v) at a feed gas rate of 2 mL min^{-1}.

ratio of 50/50, revealing a prominent separation performance for CO_2/CH_4 (see Fig. 4b). These results suggest that $[Cu_3(\mu_3\text{-OH})(PCA)_3]$ possesses great potential in capturing CO_2 from flue gas and natural gas.

Conclusions

In summary, we herein revealed the outstanding CO_2 separation performance on a metal–organic framework ($[Cu_3(\mu_3\text{-OH})(PCA)_3]$) comprising nano-cages and a high density of dual-side open metal sites. Induced by the exquisite configuration of the network and tri-nuclear secondary building units, an ultra-high density of accessible open metal sites is generated in the pore channels of $[Cu_3(\mu_3\text{-OH})(PCA)_3]$. As a result, this MOF exhibits significant differences in adsorption uptakes for CO_2/N_2 and CO_2/CH_4, making it a promising candidate for capturing CO_2 from flue gas and natural gas. Furthermore, this MOF also shows outstanding separation performance in separating CH_4 from C2–C3 light hydrocarbons. Theoretical investigation reveals that the open metal sites are preferable adsorption sites for CO_2 and C2–C3 components. Breakthrough experiments also validate the outstanding separation performance for this MOF. The results of this work will open a new way to develop functional MOFs with high separation performance.

Conflicts of interest

There are no conflicts to declare.

Acknowledgements

Notes and references

1 R. S. Haszeldine, *Science*, 2009, **325**, 1647–1652.
2 P. G. Boyd, A. Chidambaram, E. García-Díez, C. P. Ireland, T. D. Daff, R. Bounds, A. Gładysiak, P. Schouwink, S. M. Moosavi, M. M. Maroto-Valer, J. A. Reimer, J. A. R. Navarro, T. K. Woo, S. Garcia, K. C. Stylianou and B. Smit, *Nature*, 2019, **576**, 253–256.
3 M. Oschatz and M. Antonietti, *Energy Environ. Sci.*, 2018, **11**, 57–70.
4 C. A. Rowland, G. R. Lorzing, E. J. Gosselin, B. A. Trump, G. P. A. Yap, C. M. Brown and E. D. Bloch, *J. Am. Chem. Soc.*, 2018, **140**, 11153–11157.
5 L. Li, J. G. Bell, S. Tang, X. Lv, C. Wang, Y. Xing, X. Zhao and K. M. Thomas, *Chem. Mater.*, 2014, **26**, 4679–4695.
6 R. T. Yang, *Adsorbents: Adsorbents: Fundamentals and Applications*, John Wiley & Sons, Hoboken, 2003.
7 C. Liu, Y. Zhou, Y. Sun, W. Su and L. Zhou, *AIChE J.*, 2011, **57**, 645–654.
8 M. Luberti, D. Friedrich, S. Brandani and H. Ahn, *Adsorption*, 2014, **20**, 511–524.
9 Y.-T. Wang, C. McHale, X. Wang, C.-K. Chang, Y.-C. Chuang, W. Kaveevivitchai, O. Š. Miljanić and T.-H. Chen, *Angew. Chem., Int. Ed.*, 2021, **60**, 14931–14937.
10 P. Nugent, Y. Belmabkhout, S. D. Burd, A. J. Cairns, R. Luebke, K. Forrest, T. Pham, S. Ma, B. Space, L. Wojtas, M. Eddaoudi and M. J. Zaworotko, *Nature*, 2013, **495**, 80–84.
11 F. G. Kerry, *Industrial Gas Handbook: Gas separation and Purification*, CRC Press, Boca Raton, FL, 2007.
12 O. T. Qazvini, R. Babarao and S. G. Telfer, *Nat. Commun.*, 2021, **12**, 197.
13 Y. Belmabkhout, P. M. Bhatt, K. Adil, R. S. Pillai, A. Cadiau, A. Shkurenko, G. Maurin, G. Liu, W. J. Koros and M. Eddaoudi, *Nat. Energy*, 2018, **3**, 1059–1066.
14 M. K. Taylor, T. Runcevski, J. Oktawiec, J. E. Bachman, R. L. Siegelman, H. Jiang, J. A. Mason, J. D. Tarver and J. R. Long, *J. Am. Chem. Soc.*, 2018, **140**, 10324–10331.
15 Y.-S. Bae, K. L. Mulfort, H. Frost, P. Ryan, S. Punnathanam, L. J. Broadbelt, J. T. Hupp and R. Q. Snurr, *Langmuir*, 2008, **24**, 8592–8598.
16 H. Furukawa, K. E. Cordova, M. O'Keeffe and O. M. Yaghi, *Science*, 2013, 341.
17 A. Cadiau, Y. Belmabkhout, K. Adil, P. M. Bhatt, R. S. Pillai, A. Shkurenko, C. Martineau-Corcos, G. Maurin and M. Eddaoudi, *Science*, 2017, **356**, 731–735.
18 J.-R. Li, Y. Ma, M. C. McCarthy, J. Sculley, J. Yu, H.-K. Jeong, P. B. Balbuena and H.-C. Zhou, *Coord. Chem. Rev.*, 2011, **255**, 1791–1823.
19 X. Lv, L. Li, S. Tang, C. Wang and X. Zhao, *Chem. Commun.*, 2014, **50**, 6886–6889.
20 S. Su, Y. Zhang, M. Zhu, X. Song, S. Wang, S. Zhao, S. Song, X. Yang and H. Zhang, *Chem. Commun.*, 2012, **48**, 11118–11120.
21 A. Spek, *J. Appl. Crystallogr.*, 2003, **36**, 7–13.
22 Q. Min Wang, D. Shen, M. Bülow, M. Ling Lau, S. Deng, F. R. Fitch, N. O. Lemcoff and J. Semanscin, *Microporous Mesoporous Mater.*, 2002, **55**, 217–230.
23 P. Mishra, S. Edubilli, B. Mandal and S. Gumma, *Microporous Mesoporous Mater.*, 2013, **169**, 75–80.
24 A. L. Myers and J. M. Prausnitz, *AIChE J.*, 1965, **11**, 121–127.
25 M. Zhang, X. Xin, Z. Xiao, R. Wang, L. Zhang and D. Sun, *J. Mater. Chem. A*, 2017, **5**, 1168–1175.
26 K. Liu, B. Li, Y. Li, X. Li, F. Yang, G. Zeng, Y. Peng, Z. Zhang, G. Li, Z. Shi, S. Feng and D. Song, *Chem. Commun.*, 2014, **50**, 5031–5033.
27 D. Dubbeldam, S. Calero, D. E. Ellis and R. Q. Snurr, *Mol. Simul.*, 2016, **42**, 81–101.